Article

The Effects and Mechanism of Guilu Bushen Pill in the Treatment of Osteoporosis Model in Ovariectomized Rats

Ximing Peng [1], Junjie Huang [1], Peifang Lai [1], Xiaorong Zhang [1], Mingdeng Guan [1], Xin Hu [1], Yimeng Ma [1], Meiqi Ji [1], Haiyan Gong [1], Chunhong Li [1], Xiuping Chen [2], and Huaqian Wang [1,*]

[1] School of Biomedical and Pharmaceutical Sciences, Guangdong University of Technology, Guangzhou 510006, China
[2] State Key Laboratory of Quality Research in Chinese Medicine, Institute of Chinese Medical Sciences, University of Macau, Macao 519000, China
* Correspondence: hqwang@gdut.edu.cn

Abstract: Guilu Bushen Pill (GLBSW) is a traditional Chinese medicine formulation recognized for its kidney-nourishing effects. According to traditional Chinese medicine theory, kidney health is closely linked to bone strength. This study aims to investigate the effects of GLBSW on osteoblast differentiation using SaoS-2 cells, as well as its therapeutic potential in an ovariectomy-induced osteoporosis (OVX) rat model. In vitro results indicate that GLBSW significantly promotes the differentiation of SaoS-2 cells, while in vivo experiments demonstrate its effectiveness in alleviating osteoporosis in OVX rats by enhancing bone mineral density (BMD), improving both the quantity and quality of bone trabeculae, and maintaining calcium and phosphorus levels in bone. Metabolomic analysis of serum metabolites suggests that the therapeutic effects of GLBSW may be associated with the modulation of pyruvate and arachidonic acid metabolism. In conclusion, these findings underscore the potential of GLBSW in the treatment of osteoporosis through the regulation of bone formation and energy metabolism.

Keywords: Guilu Bushen Pill; osteoporosis; metabolomics; ovariectomized rat

1. Introduction

Osteoporosis and related fractures are prevalent chronic metabolic bone conditions that significantly impact global health. Given the aging population, the proportion of individuals over 50 is predicted to increase from 24% in 2010 to 48% by 2050, correlating with a higher incidence of osteoporosis-related fractures in postmenopausal women [1]. This rising prevalence of osteoporosis has driven the expansion of the osteoporosis medication market [2]. Currently, pharmacological treatment is the primary therapeutic interventions, including calcium and vitamin D supplements, calcitonin, bisphosphonates, and estrogens. However, these treatments, particularly hormone therapy, are often associated with side effects, such as increased risks of myocardial infarction, gastrointestinal adverse reactions, endometrial hyperplasia, cancer, and thrombosis [3]. In comparison to conventional pharmaceuticals, traditional Chinese medicine shows greater efficacy in alleviating clinical symptoms by regulating metabolic processes, with fewer side effects and lower costs [4]. In preliminary investigations, three collagen-rich TCM formulations—Guilu Bushen Pill (GLBSW), Guilu Erxian Jiao, and Ejiao Huangqi Oral Solution—were assessed for clinical efficacy in treating osteoporosis [5]. The meta-analysis revealed significant improvements in patients receiving either single TCM formulations or a combination with conventional osteoporosis treatments, compared to those without pharmacological intervention. Furthermore, these patients showed increased bone mineral density (BMD) relative to untreated individuals [6].

In recent years, metabolomics has become an essential tool for assessing the therapeutic effects of

various TCMs [7, 8]. By collecting comprehensive metabolite profiles, metabolomic fingerprinting enables the analysis of all metabolic reactions after stimulation, providing valuable insights into the underlying mechanisms of action.

This study seeks to explore the anti-osteoporotic effects and mechanisms of Guilu Bushen Pill (GLBSW) using liquid chromatography-mass spectrometry.

2. Materials and Methods

2.1. Materials

The GLBSW was prepared by extracting a mixture of sixteen traditional Chinese medicine components (*Semen Cuscutae* 51 g, *Epimedii Folium* (steamed) 43 g, *Dipsaci Radix* (steamed with salt) 43 g, *Cynomorii Herba* (steamed) 51 g, *Cibotii Rhizoma* (steamed with salt) 64 g, *Ziziphi Spinosae Semen* (fried) 43 g, *Polygoni Multiflori Radix* 64 g, *Glycyrrhizae Radix et Rhizoma* 21 g, *Citri Reticulatae Pericarpium* 21 g, *Colla Cornus Cervi* (fried) 9 g, *Rehmanniae Radix* 64 g, *Carapax et Plastrum Testudinis Colla* (fried) 13 g, *Rosae Laevigatae Fructus* (steamed) 51 g, *Astragali praeparata cum Melle Radix* 43 g, *Yams* (fried) 43 g, *Rubi Fructus* (steamed) 85 g), which was a gift from Guangzhou Baiyunshan Huacheng Pharmaceutical Limited Company. (Guangzhou, China). 17 β-estradiol (E2) was purchased from Bayer Healthcare Co., Ltd. (Shanghai, China). Enzyme-linked immunosorbent assay (ELISA) kits for PY, TRAP, ALP and BGP were purchased from Nanjing Jiancheng Bioengineering Institute (Nanjing, China).

2.2. Cell Culture

SaoS-2 cells obtained from ATCC (Manassas, VA, USA) were cultured in DMEM, supplemented with 10% fetal bovine serum, 100 units/mL penicillin and 0.1 mg/mL streptomycin. The cells were incubated in a humidified atmosphere of 95% air and 5% CO_2 at 37 ℃.

2.3. ALP Activity Assay

The SaoS-2 cells (5×10^5 cells/well) were initially seeded into 6-well plates. After a 24-h incubation period, the cell medium was replaced with osteogenic induction medium, containing 50 μg/L ascorbic acid, 10 mmol/L β-sodium glycerophosphate, 1×10^{-8} mmol/L dexamethasone, and with different concentrations of GLBSW. After 7 days of incubation, the cell supernatant was collected for alkaline phosphatase (ALP) activity detection using the alkaline phosphatase assay kit (Nanjing Jiancheng Bioengineering Institute, Nanjing, China). The protein content was determined using the Bicinchoninic Acid Assay kit (Beyotime Biotechnology Co. Ltd., Shanghai, China).

2.4. Alizarin Red S Staining

The cultivation and intervention of SaoS-2 cells for Alizarin Red staining (ARS) followed procedures similar to those detailed in Section 2.3. After 14 days of induction, the cells were fixed with 4% paraformaldehyde (PFA) for 20 min. ARS staining was performed using the ARS kit (Sigma-Aldrich, St. Louis, MI, USA) to observe the formation of mineralized nodules.

2.5. Animal Experiment

Eight-month-old SD female rats were obtained from the Guangdong Medical Laboratory Animal Center (Guangdong, China), with an animal certificate number of SYXK (YUE) 2017-0215. The animal experiments were conducted at the Animal Experiment Center of Guangdong Pharmaceutical University (Guangzhou, China). All the animal experiments involved had been reviewed and approved by the ethics committee of experimental animals of Guangdong University of Technology (Ethical review number: JN. No GDUTXS2023219).

After two weeks of adaptive feeding, the SD female rats (n = 42) underwent either bilateral laparotomy (sham, n = 7) or bilateral ovariectomy (OVX, n = 35). All rats were located in padded cages where they could have free access to chow and water (temperature: 18–22 ℃, humidity: 40–60%). One week after surgery, the rats were randomly assigned to five groups, each comprising seven rats and the groups received different

treatments by intragastric administration: OVX group, estradiol valerate (EV) group, 0.81 g/kg/d GLBSW-L group, 1.62 g/kg/d GLBSW-M group and 3.24 g/kg/d GLBSW-H group. The rats were sacrificed after 3 months of treatment.

2.6. Bone Micro-CT Measurement

The left femurs were fixed with 10% formalin for bone parameter analysis and then were scanned using a high-resolution cone beam micro-CT system (Milabs B.V). The X-ray energy level was set to 50 kV and 200 μA, with a pixel size of 8.9 μm, an aluminum (Al) filter thickness of 0.5 mm, and a rotation angle of 180° with rotation steps of 0.4°. Datasets were reconstructed using MILabs Rec 10.16 software and were further evaluated using IMALYTICS software. After that, the region of interest (ROI) in the bone tissue, located 1.0 mm distal to the growth plate, was selected for analysis.

2.7. Bone Mechanical Parameters Measurement

After micro-CT measurement, the femur bone tissues in each group were evaluated using a three-point-bending test, which was conducted with an electronic dynamic and static testing machine (Hegewald & Peschke, Nossen, Germany), with a 20 mm gap.

2.8. Analysis of Bone Mineral Contents

The fractured femurs were collected and the ash contents in the bones were measured using the muffle furnace method. The contents of inorganic matter (calcium and phosphorus) in bone ash were measured by EDTA titration and UV photometer respectively [9].

2.9. Serum Bone Turnover Markers Detection

Blood samples were collected. Subsequently, serum concentrations of ALP (MLBIO, Shanghai, China, ml003150-2), BGP (MLBIO, Shanghai, China, ml002883-2), PY (MLBIO, Shanghai, China, ml003150-2), and TRAP (MLBIO, Shanghai, China, ml306452-2) were measured using a microplate reader (Thermo, Multiskan, FC, Waltham, MA, USA) according to the protocols listed on the ELISA kits.

2.10. Hematoxylin and Eosin Staining

The femur tissues were fixed in formalin for 24 h, then immersed in a 10% EDTA solution (pH 8.0) and subsequently placed on a lab shaker at 4 ℃. After 8 weeks, the softened femur tissues underwent gradient ethanol dehydration, initially immersed in xylene for 25 min and subsequently in wax for 3 h. The tissues were then paraffin-embedded and sectioned at 5 μm thickness by Leica tissue slicer (Leica RM2235, Wetzlar, Germany). Finally, hematoxylin and eosin (H&E) staining was performed according to the manufacturer's protocol.

2.11. Metabolomic Analysis

High-resolution accurate mass liquid chromatography-tandem mass spectrometry (HRAM LC-MS/MS) analysis was conducted using a Thermo Scientific Ultimate 3000 RSLC and a Q Exactive Orbitrap desktop high-resolution mass spectrometer was performed using Thermo Scientific Xcalibur software. Compound Discoverer 2.1 along with the mzCloud database (Thermo Scientific, http://www.mzcloud.org, accessed on 20 February 2023) was used for data analysis. Liquid-phase separation employed a Hypersil GOLD C18 column (100 × 2.1 mm, 1.9 μm) at a column temperature of 40 ℃, with an injection volume of 2 μL and a flow rate of 0.3 mL/min. The mobile phase consisted of phase A (0.1% formic acid in water) and phase B (methanol solution). The gradient elution sequence was set as follows: 0 min, 2% B; 2 min, 2% B; 5 min, 20% B; 12 min, 95% B; 17 min, 95% B; 17.1 min, 2% B; 20 min, 22% B. For MS/MS analysis, the ion source was set to H-ESI, and the scan mode was Full MS-ddMS2, with a full MS scan range of 70–1000 m/z, resolution of 70,000 FWHM, and an isolation width of 0.4 m/z. The mass spectrometer spray voltage ranged from 4.0 to 3.0 kV, capillary temperature was set at 320 ℃, and the auxiliary gas heater temperature was set at 350 ℃. Additionally, Compound Discoverer 2.1 and SIMCA software 14.1 were utilized for data analysis to measure

statistical differences in metabolites between groups. MetaboAnalyst (accessible athttps://www.metaboanalyst.ca/) was employed to enrich the metabolic pathways of significantly different metabolites.

2.12. Statistical analysis

The data are presented as the mean ± standard deviation. Student's t-test was employed to analyze intergroup differences, and one-way analysis of variance (ANOVA) using GraphPad Prism 7 (GraphPad Software, La Jolla, CA, USA) was utilized to compare data among more than two groups. The significance level was set at $p < 0.05$.

3. Results

3.1. GLBSW Promotes the Osteogenic Differentiation Activity of SaoS-2 Cells

Alkaline phosphatase (ALP) plays a critical role in bone formation. To evaluate the effects of GLBSW on the osteogenic differentiation of SaoS-2 cells, ALP activity was measured after 72 h of treatment. As shown in Figure 1A, ALP activity significantly increased ($p < 0.05$) in cells treated with 0.5 and 1 μg/mL of GLBSW, indicating a marked enhancement of osteogenic differentiation. To further investigate the relationship between ALP activity and bone mineralization, SaoS-2 cells underwent 14 days of osteogenic induction, followed by the assessment of calcium deposition. As depicted in Figure 1B, treatment with 1 μg/mL of GLBSW significantly enhanced calcium deposition ($p < 0.01$). Additionally, Figure 1C illustrates a positive correlation between calcium deposition and GLBSW concentration, confirming the role of GLBSW in promoting mineralization in SaoS-2 cells.
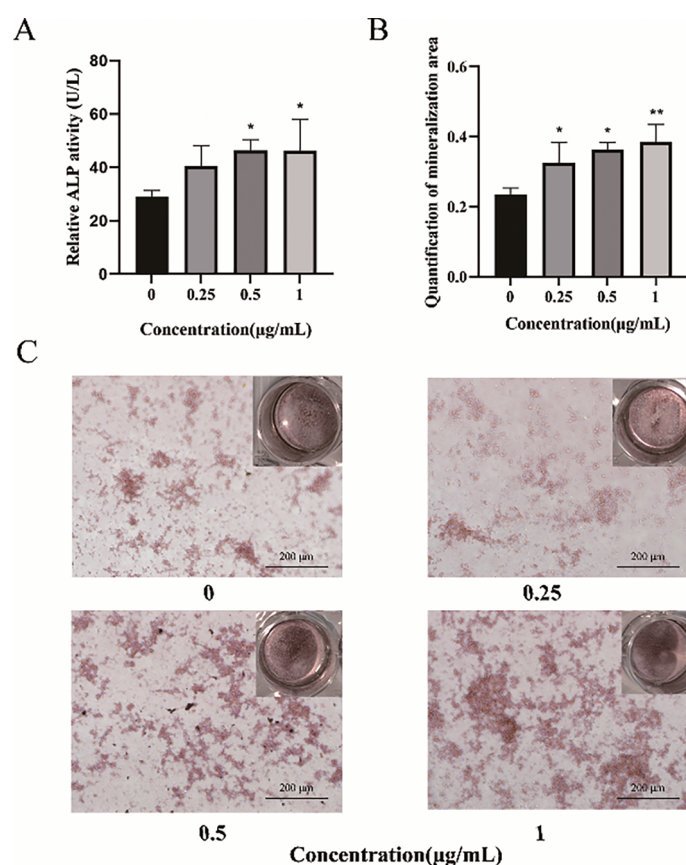

Figure 1. GLBSW enhances osteogenic differentiation in SaoS-2 cells. (**A**) Effect of GLBSW on ALP activity in SaoS-2 cells after 7 days. (**B**) Analysis of ARS staining in SaoS-2 cells following 14 days of GLBSW treatment. (**C**) ARS staining images of SaoS-2 cells treated with GLBSW (100×) after 14 days. * $p < 0.05$, ** $p < 0.01$ compared to the control group.

3.2. GLBSW Enhance Bone Mass in OVX

To investigate the effects of GLBSW in an ovariectomy-induced osteoporosis (OVX) model, we utilized micro-computed tomography (Micro-CT) to assess bone quality and therapeutic outcomes. As shown in Figure 2A, the OVX group exhibited trabecular bone loss, characterized by deteriorated trabecular network and decreased cortical bone thickness compared to the sham group. In contrast, both the EV and GLBSW groups demonstrated substantial improvements in bone structure. Figure 2B indicates that Micro-CT analysis of the OVX group showed significant decreases in bone volume fraction (BV/TV), bone mineral density (BMD), trabecular number (Tb.N) and trabecular thickness (Tb.Th) $(p < 0.001)$, along with marked increases in bone surface density (BS/TV) and trabecular separation (Tb.Sp) $(p < 0.001)$, confirming the successful induction of the osteoporosis model. Notably, both the EV and GLBSW groups showed improvements in these parameters, including increases in cortical bone thickness post-treatment compared to the OVX group. The results showed that the GLBSW has similar efficacy to EV which is already used in the clinical treatment of osteoporosis. These findings suggest that GLBSW has the potential to enhance BMD and improve trabecular bone structure. In summary, GLBSW has the ability to improve the trabecular bone structure in OVX rats.
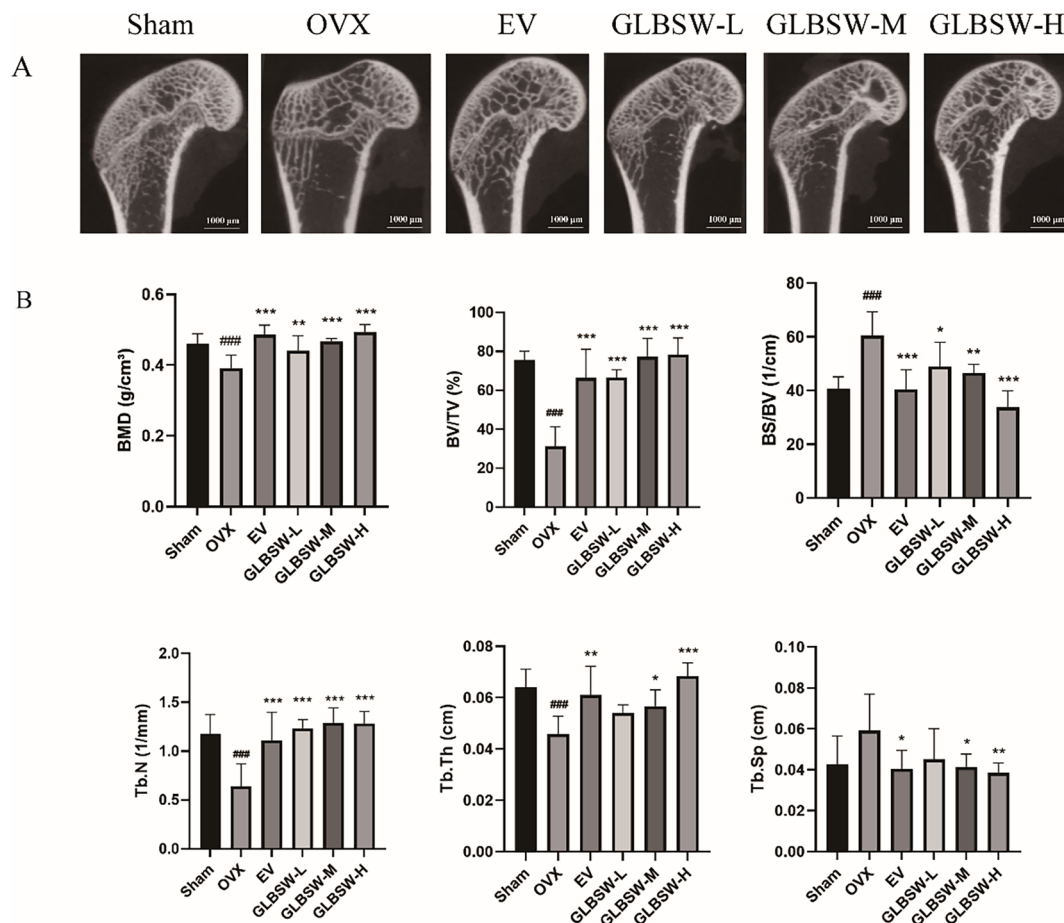

Figure 2. Images of femur and bone micro-CT parameters in different groups after 3 months of GLBSW treatment. (**A**) Images of femur metaphysis in each group. (**B**) Bone micro-CT parameters of each group. ### $p < 0.001$ compared with the sham group. * $p < 0.05$, ** $p < 0.01$, *** $p < 0.001$ compared with the OVX group, n = 7 for each group.

3.3. GLBSW Improves Tibia Strength and Enhances Calcium and Phosphorus Content in OVX

As shown in Figure 3A, B, both the maximum tensile stress and flexural strength of the tibia were significantly higher in the EV and GLBSW groups compared to the OVX group. Additionally, Figure 3C, D illustrate that calcium and phosphorus levels in the tibiae of the sham, EV, and GLBSW groups were restored to normal levels, which were reduced in the OVX group. Furthermore, Figure 3E, F indicate no significant differences in the length and diameter of the rat femurs among the groups.
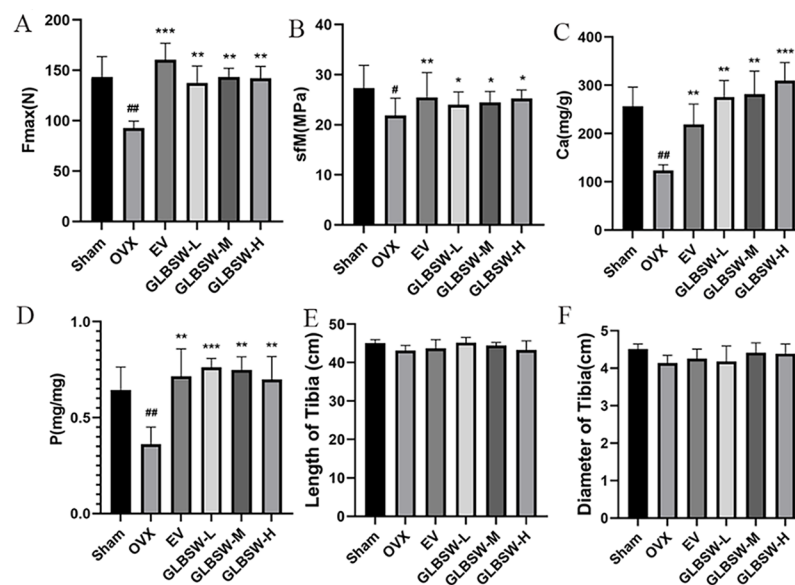
Figure 3. Effects of GLBSW on tibia strength and the content of calcium and phosphorus in rats. (**A**) Fmax: Maximum stress of tibia. (**B**) sfM: Flexural strength of the tibia. (**C**) Effects of GLBSW on the calcium content of bone in OVX rats. (**D**) Effects of GLBSW on the phosphorus content of bone in OVX rats. (**E**) Length of the rat femur. (**F**) Diameter of the rat femur. [#] $p < 0.05$, [##] $p < 0.01$ compared with the sham group, * $p < 0.05$, ** $p < 0.01$, *** $p < 0.001$ compared with the OVX group.

3.4. Effect of GLBSW on Bone Metabolism in Serum of Rats

PY reflects bone resorption and collagen degradation, while TRAP indicates bone resorption, and ALP and BGP are biomarkers of bone formation. As shown in Figure 4, serum levels of TRAP and PY significantly decreased in all treatment groups compared to the OVX group, while BGP and ALP levels significantly increased. These findings suggest that GLBSW not only promotes bone formation and inhibits bone resorption, thereby mitigating osteoporosis, but also reduces serum collagen degradation related to collagen absorption from GLBSW.
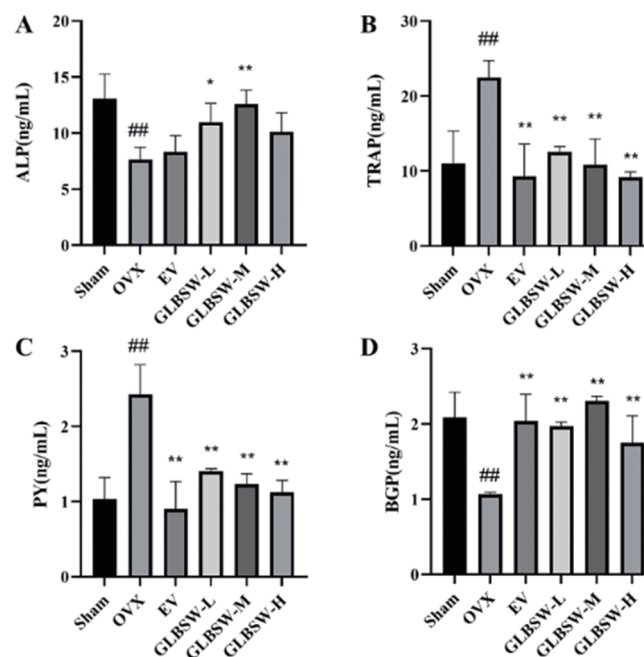

Figure 4. Changes in serum bone metabolism markers in each group after 3 months of GLBSW treatment. (**A**) Levels of serum ALP; (**B**) Levels of serum TRAP; (**C**) Levels of serum PY; (**D**) Levels of serum BGP. * $p < 0.05$, ** $p < 0.01$ compared with the OVX group, [##] $p < 0.01$ compared with the sham group, n = 7 for each group.

3.5. Effects of GLBSW on Bone Histomorphology in Rats

The right femur was fixed in formalin, embedded in paraffin, sectioned, stained with hematoxylin and eosin (HE), and subsequently examined under a microscope for tissue changes. As shown in Figure 5, the femur in the sham group exhibited a normal structure, characterized by dense, uniform trabecular architecture and good continuity. In contrast, the OVX group displayed fractures, thinning, and widened trabecular gaps in the distal femur. The EV and GLBSW groups, however, only exhibited minor trabecular fractures and slight widening of trabecular spaces. Compared to the OVX group, bone loss was less severe in the EV and GLBSW groups, with partial restoration of trabecular structure and spacing, particularly in the high-dose GLBSW (GLBSW-H) group, demonstrating its anti-osteoporotic efficacy.
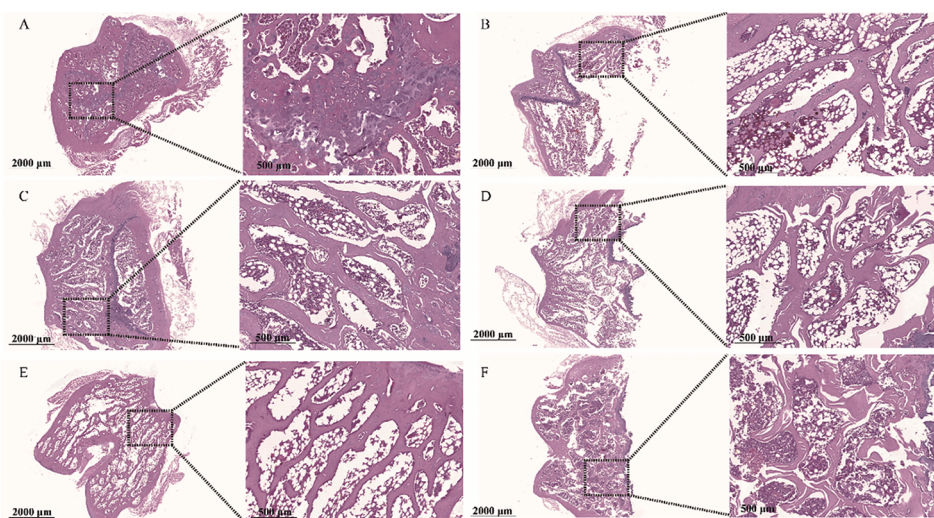

Figure 5. HE staining of rat femoral tissue sections. (**A**)–(**F**): Sham Group, OVX Group, EV Group, GLBSW-L Group, GLBSW-M Group, GLBSW-H Group.

3.6. Metabolic Analysis of the Effect of GLBSW on Osteoporosis in OVX

Principal Component Analysis (PCA), Partial Least Squares Discriminant Analysis (PLS-DA), and Orthogonal-Partial Least Squares Discriminant Analysis (OPLS-DA) were performed using Compound Discoverer 2.0 software and SIMCA software 14.1. As shown in Figure 6A – J, the sham and OVX groups exhibited complete separation in the serum metabolic profiles, indicating significant changes in the serum metabolism in the OVX model. Additionally, the metabolic profiles of the GLBSW-L, GLBSW-M and GLBSW-H groups also showed noticeable separation from the OVX group, consistent with the results from the in vivo experiments. These findings further highlight the significant impact of GLBSW on rat serum metabolites.

Variable Importance in Projection (VIP) values from OPLS-DA analysis were obtained to assess intergroup differences. Subsequently, fold change (FC) in metabolite expression between the OVX group and other groups was calculated using Compound Discoverer 2.0 software and converted to log2FC values. Differential metabolites were then identified based on VIP and log2FC values, with metabolites deemed significantly different if they met the criteria of VIP > 1 and log2FC $\geq$ 0.263 (or log2FC $\leq$ − 0.5778). Identified differential metabolites are shown in Tables 1 and 2.

To identify metabolic pathways associated with osteoporosis, differential metabolites were analyzed using the MetaboAnalyst 5.0 online platform. As shown in Table 3, eight potential pathways with impact values greater than 0.1 were identified, including pyruvate metabolism (0.18519) and arachidonic acid metabolism (0.11111). Prostaglandin E2, thromboxane B1, 13-Hpode (1-), and Ent-8-iso prostaglandin F2α were notably downregulated in the GLBSW low-, medium-, and high-dose groups but upregulated in the OVX group (Tables 1 and 2), suggesting GLBSW may normalize serum biomarkers associated with osteoporosis, thereby correcting systemic metabolic disorders. Consequently, GLBSW administration in rats is suggested to inhibit serum ketone and arachidonic acid metabolism, contributing to the amelioration of osteoporosis.
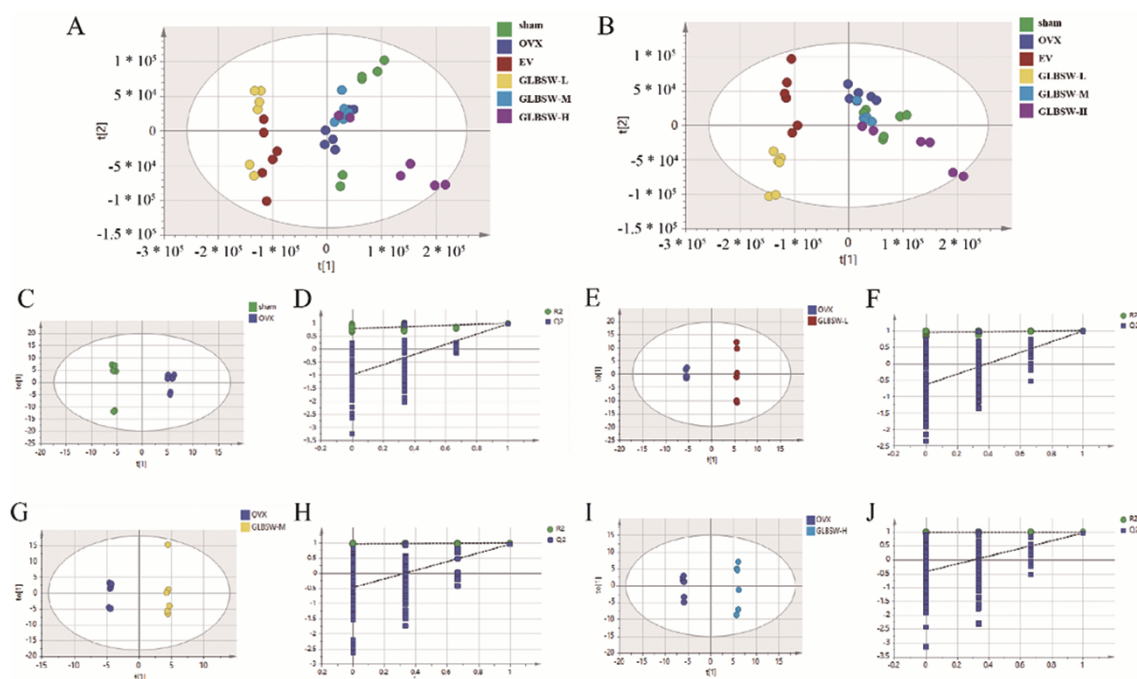
Figure 6. Metabolomics model analysis. (**A**) PCA score plot of OVX rat serum; (**B**) PLS-DA score plot of OVX rat serum; (**C,E,G,I**). OPLS-DA analysis; (**D,F,H,J**). Permutation tests for OPLS-DA.

Table 1. $\log_2$FC of serum metabolites in OVX rats.

Name	RT [min]	Sham vs. OVX	GLBSW-L vs. OVX	GLBSW-M vs. OVX	GLBSW-H vs. OVX
13-Hpode (1-)	12.205	−1.3	−0.83	−1.12	−1.47
15(S)-HpETE	12.558	−1.32	−1.19	−0.62	−1.13
ent-8-iso Prostaglandin F2α	12.557	−1.22	−0.77	−0.73	−1.07
Phenylacetylglycine	4.892	0.76	−7.57	−0.61	−0.74
(15Z)-9,12,13-Trihydroxy-15-octadecenoic acid	12.207	−1.38	−0.83	−0.65	−0.68
12-Epileukotriene B4	14.967	0.77	−0.54	−0.4	−0.57
15(S)-HpETE	13.882	−0.8	−1.47	−0.89	−0.47
Uric acid	1.088	0.99	−3.08	−0.77	−0.47
Prostaglandin E2	13.258	−1.09	−0.87	−0.52	−0.46
Thromoboxane B1	12.558	−1.09	−0.78	−0.54	−0.38
D-Malic acid	0.959	−0.41	8.75	−0.35	−0.33
L-Malic acid	0.959	−0.41	8.75	−0.35	−0.33
Taurochenodeoxycholic acid	12.462	0.8	0.94	−0.9	0.65
Dibenzylamine	9.448	−1.93	−7.43	2.59	1.16
Erucamide	17.805	−0.84	1.84	0.96	1.4
NP-021797	16.686	−2.51	1.37	1.15	1.42
Dibutyl phthalate	14.132	−0.69	0.75	1.45	1.46
Docosanamide	18.282	−1.76	1.99	2.98	2.11
Docosahexaenoic acid ethyl ester	13.025	−1.76	2.29	0.69	2.14
Azelaic acid	15.427	−3.48	4.07	4.19	2.29
D-Lactic Acid	0.913	−3.03	3.46	2.25	3.02
L-Lactic Acid	0.913	−3.03	3.46	2.25	3.02

Table 2. VIP of serum metabolites in OVX rats.

Name	HMDB	Pubchem	KEGG	Sham vs. OVX	GLBSW-L vs. OVX	GLBSW-M vs. OVX	GLBSW-H vs. OVX
13-HpODE(1-)	HMDB0062637	1426	–	0.6048	0.3448	0.9678	0.7576
15(S)-HpETE	HMDB0004244	5,280,893	C05966	0.6055	0.1847	0.6625	1.0994
ent-8-iso Prostaglandin F2α	HMDB0005083	5,282,263	C13809	1.0034	0.8967	0.6865	0.1716
Phenylacetylglycine	HMDB0000821	68,144	C05598	0.9705	1.6656	1.0101	0.9299
(15Z)-9,12,13-Trihydroxy-15-octadecenoic acid	HMDB0035919	44,559,173	–	0.8133	0.5329	0.7818	0.5100
12-Epileukotriene B4	HMDB0005088	5,283,129	–	0.4540	0.0307	0.6335	0.5481
15(S)-HpETE	HMDB0004244	5,280,893	C05966	0.6055	0.1847	0.6625	1.0994
Uric acid	HMDB0000289	1175	C00366	1.2214	1.9638	2.0631	1.4100
Prostaglandin E2	HMDB0001220	5,283,116	C00584	1.5593	0.8110	0.5647	0.1225
Thromoboxane B1	HMDB03252	5,283,137	C05963	0.8952	0.9852	0.6284	0.2008
D-Malic acid	HMDB0031518	92,824	C00497	0.4525	1.9103	0.6001	0.8630
L-Malic acid	HMDB0000156	222,656	C00149	0.4525	1.9103	0.6001	0.8630
Taurochenodeoxycholic acid	HMDB0000951	387,316	C05465	0.2421	1.0161	0.7906	0.3691
Dibenzylamine	HMDB0251169	7656	–	0.9741	1.3352	1.8633	0.3346
Erucamide	HMDB0244507	8214	–	0.4842	1.4639	1.1108	1.4690
NP-021797	HMDB0340656	101, 766,552	–	1.1884	1.6755	1.9125	1.5373
Dibutyl phthalate	HMDB0033244	3026	C14214	0.7906	0.7076	1.5080	1.2159
Docosanamide	HMDB0000583	76,468	–	0.4300	0.3307	1.7076	0.6835
Docosahexaenoic acid ethyl ester	HMDB0251557	150,680	–	0.6169	1.1895	1.0318	1.3101
Azelaic acid	HMDB0000784	2266	C08261	0.8942	1.0547	0.5911	1.2851
D-Lactic Acid	HMDB0001311	61,503	C00256	2.0283	1.9326	1.6775	1.8231
L-Lactic Acid	HMDB0000190	61,503	C00186	2.0283	1.9326	1.6775	1.8231

Table 3. Metabolic pathways enriched in serum of OVX rats.

Metabolic Pathways	Hits	Raw *p*	Pathway Impact	Details
Pyruvate metabolism	3	0.000145	0.18519	KEGG SMP
Arachidonic acid metabolism	2	0.014215	0.11111	KEGG SMP
Phenylalanine metabolism	1	0.062136	0.0	KEGG SMP
Citrate cycle (TCA cycle)	1	0.10166	0.06897	KEGG
Glycolysis / Gluconeogenesis	1	0.13034	0.02857	KEGG SMP SMP
Glyoxylate and dicarboxylate metabolism	1	0.15821	0.03846	KEGG
Primary bile acid biosynthesis	1	0.22023	0.0	KEGG SMP
Purine metabolism	1	0.30188	0.01136	KEGG SMP

4. Discussion

GLBSW, a traditional formula from *"Qian Jin Yao Fang"*, is included in the 2020 edition of the *"Chinese Pharmacopoeia"*. Known for its kidney-nourishing, qi-tonifying, and blood-replenishing properties, GLBSW employs a multi-target approach in treating postmenopausal osteoporosis. Its components can improve circulation, promote bone resorption, prevent bone loss, and influence bone metabolism. Given its diverse active ingredients, GLBSW is predicted to have therapeutic potential for osteoporosis. However, current research primarily focuses on male sexual dysfunction and female ovulation

disorders, with limited studies on osteoporosis. This study, using an OVX rat model, demonstrated that GLBSW significantly alleviates osteoporosis, highlighting its therapeutic potential, particularly for elderly populations due to its multi-component, systemic regulatory properties.

Studies have shown that various components of GLBSW, such as *Semen Cuscutae*, *Epimedium*, *Radix Dipsaci*, and *Cynomorium*, can promote osteoblast differentiation and inhibit osteoclast resorption [10–14]. Additionally, *Semen Cuscutae*, *Radix Dipsaci*, and *Cynomorium* have demonstrated significant anti-osteoporotic effects in OVX rats [15–18]. These herbs primarily promote osteoblast formation through signaling pathways including BMP-Smads, Wnt/β-catenin, MAPK, and PI3K/AKT, while inhibiting bone resorption via the OPG/RANKL/RANK and estrogen signaling pathways [19,20]. For instance, *Radix Dipsaci* upregulates the expression of P-Smad1/5/8, P-ERK1/2, P-p38, and Runx2 [12], whereas Cynomorium downregulates NF-κB and PI3K/AKT signaling via the RANKL/RANK/TRAF6 pathway. Both in vivo and in vitro studies have shown that *Cibotium* and *Cornus Cervi Colla* improve bone metabolism and alleviate the imbalance between bone formation and resorption [21,22]. W.Q. Kang et al. found that *Radix Rehmanniae Preparata* combined with *Astragali Radix* may treat osteoporosis by activating the PI3K/AKT pathway [23]. Moreover, J.H. Hwang et al. found that yam-derived exosome-like nanovesicles promote osteogenesis via the BMP-2/p-p38/Runx2 pathway [24]. Additionally, *Polygoni Multiflori Radix* significantly inhibits RANKL-induced osteoclast differentiation by suppressing NFATc1 transcription and translation, highlighting its anti-osteoporotic effects [16,25]. In this study, GLBSW treatment significantly lowered serum TRAP and PY levels in OVX rats while increasing BGP and ALP levels, with ALP being a key marker of osteoblast differentiation regulated by BMP-Smads and Wnt/β-catenin. These results suggest that GLBSW may exert its effects through these pathways, though further research is needed to elucidate its mechanisms.

Pyruvate metabolism, the final pathway of nutrient processing, generates substantial ATP through the mitochondrial respiratory chain, which provides the essential energy for osteoblasts during bone formation [26]. Studies have demonstrated that metabolic regulation, particularly a moderate increase in pyruvate levels, significantly enhance osteoblast function. In this study, metabolomic analysis revealed that GLBSW can modulate the pyruvate metabolic pathway, potentially exerting therapeutic effects on osteoporosis by regulating energy metabolism. Furthermore, metabolic profiling revealed significant changes in serum levels of cyclooxygenase (COX) and prostaglandins following GLBSW administration. In kidney deficiency model rats, additional metabolic analysis indicated that *Semen Cuscutae* affects arachidonic acid metabolism [6], while *Epimedium* exerts anti-osteoporotic effects by modulating 11 estrogen-related signaling pathways [27]. Arachidonic acid metabolism encompasses three main pathways, facilitated by enzymes such as cyclooxygenase (COX), lipoxygenase (LOX), and cytochrome P450 (CYP450), generating a range of bioactive mediators [28]. COX pathway, the first identified metabolic route for arachidonic acid, catalyzes the formation of prostaglandins (PGs) and thromboxane A2 (TXA2) via COX-2 (PTGS2) and COX-1 (PTGS1). Therefore, the anti-osteoporotic effects of GLBSW may be attributed to its regulation of energy and bone metabolism pathways.

5. Conclusions

This study aims to evaluate the efficacy of GLBSW as a combination therapy for osteoporosis, thereby establishing a pharmacological foundation for the comprehensive exploration of its active components.

Author Contributions: H.W., X.C. and X.P. conceptualized and planned the experiments. X.P., X.Z., M.G., J.H., P.L., M.J., and H.G. performed most of the experiments and completed the original draft. X.P., M.J., H.G. and H.W. analyzed the data. H.W., X.C. and X.P. check the figures and spelling. X.P., X.Z., M.G., J.H., P.L., X.H., Y.M. and C.L. raised the animals. All authors have read and agreed to the published version of the manuscript.

Institutional Review Board Statement: The study was conducted in accordance with the guidelines for the care and use of laboratory animals and was approved by the Experimental Animal Ethics Committee of Guangdong University of Technology.

Informed Consent Statement: Not applicable.

Data Availability Statement: Not applicable.

Acknowledgments: We would like to express our heartfelt appreciation to Lvdan Zeng for her assistance with language editing and proofreading.

Conflicts of Interest: The authors declare no conflict of interest.

References

1. Lim, V. A practical approach to secondary osteoporosis e Case studies in Asia. *Osteoporosis Sarcopenia* **2016**, *2*, 134–139. https://doi.org/10.1016/j.afos.2016.07.003.

2. Amin, U.; McPartland, A.; O'Sullivan, M.; et al. An overview of the management of osteoporosis in the aging female population. *Womens Health* **2023**, *19*, 17455057231176655. https://doi.org/10.1177/17455057231176655.

3. Brennan, A.; Rees, M. Menopausal hormone therapy in women with benign gynaecological conditions and cancer. *Best Pract. Res. Clin. Endoc. Metab.* **2021**, *35*, 9. https://doi.org/10.1016/j.beem.2021.101575.

4. Slupski, W.; Jawien, P.; Nowak, B. Botanicals in Postmenopausal Osteoporosis. *Nutrients* **2021**, *13*, 27. https://doi.org/10.3390/nu13051609.

5. Fan, K.X.; Chen, X.X.; He, X.Y.; et al. Meta analysis of three kinds of collagen-rich traditional Chinese medicine compound in the treatment of osteoporosis. *Chin. J. Osteoporos.* **2021**, *27*, 1745–1751. https://doi.org/10.3969/j.issn.1006-7108.2021.12.005.

6. Fan, R.H.; Liu, C.G.; Zhang, Z.; et al. Metabolomics analysis of Semen Cuscutae protection of kidney deficient model rats using ultra high-performance liquid chromatography-quadrupole time-of-flight Mass Spectrometry. *J. Pharm. Biomed. Anal.* **2022**, *207*, 114432. https://doi.org/10.1016/j.jpba.2021.114432.

7. Chen, D.Q.; Cao, G.; Chen, H.; et al. Identification of serum metabolites associating with chronic kidney disease progression and anti-fibrotic effect of 5-methoxytryptophan. *Nat. Commun.* **2019**, *10*, 15. https://doi.org/10.1038/s41467-019-09329-0.

8. Wang, M.; Chen, L.; Liu, D.; et al. Metabolomics highlights pharmacological bioactivity and biochemical mechanism of traditional Chinese medicine. *Chem. Biol. Interact.* **2017**, *273*, 133–141. https://doi.org/10.1016/j.cbi.2017.06.011.

9. Gonzalez-Reimers, E.; Martinez-Riera, A.; Santolaria-Fernandez, F.; et al. Relative and combined effects of ethanol and protein deficiency on zinc, iron, copper, and manganese contents in different organs and urinary and fecal excretion. *Alcohol* **1998**, *16*, 7–12. https://doi.org/10.1016/s0741-8329(97)00156-0.

10. Dai, W.R.; Sun, Y.; Zhong, G.Q. A Network Pharmacology Approach to Estimate the Active Ingredients and Potential Targets of Cuscutae semen in the Treatment of Osteoporosis. *Med. Sci. Monitor* **2020**, *26*, 20. https://doi.org/10.12659/msm.920485.

11. Liu, Z.G.; Zhang, R.; Li, C.; et al. The osteoprotective effect of Radix Dipsaci extract in ovariectomized rats. *J. Ethnopharmacol.* **2009**, *123*, 74–81. https://doi.org/10.1016/j.jep.2009.02.025.

12. Niu, Y.B.; Kong, X.H.; Li, Y.H.; et al. Radix Dipsaci total saponins stimulate MC3T3-E1 cell differentiation via the bone morphogenetic protein-2/MAPK/Smad-dependent Runx2 pathway. *Mol. Med. Rep.* **2015**, *11*, 4468–4472. https://doi.org/10.3892/mmr.2015.3249.

13. Wong, R.W.K.; Rabie, A.B.M.; Hägg, E.U.O. The effect of crude extract from Radix Dipsaci on bone in mice. *Phytother. Res.* **2007**, *21*, 596–598. https://doi.org/10.1002/ptr.2126.

14. Lv, Y.; Wu, H.S.; Hong, Z.H.; et al. Exploring active ingredients of anti-osteoarthritis in raw and wine-processed Dipsaci Radix based on spectrum-effect relationship combined with chemometrics. *J. Ethnopharmacol.* **2023**, *309*, 12. https://doi.org/10.1016/j.jep.2023.116281.

15. Kim, J.H.; Kim, H.S.; Jun, J.Y.; et al. Effects of Cuscutae Semen Extract on Prevention of Osteoporosis in Ovariectomized Rats. *J. Korean Orient. Obstet. Gynecol.* **2012**, *25*, 1–11.

16. Kim, K. -J.; Yongjin, L.; Kyung-yun, K.; et al. Extracts of Polygonum multiflorum Inhibit RANKL-mediated Osteoclast Differentiation. *Yakhak Hoeji* **2018**, *62*, 83–88. https://doi.org/10.17480/psk.2018.62.2.83.

17. Ma, X.Q.; Liu, J.J.; Yang, L.L.; et al. Cynomorium songaricum prevents bone resorption in ovariectomized rats through RANKL/RANK/TRAF6 mediated suppression of PI3K/AKT and NF-κB pathways. *Life Sci.* **2018**, *209*, 140–148. https://doi.org/10.1016/j.lfs.2018.08.008.

18. Yang, Y.; Wei, Q.; An, R.; et al. Anti-osteoporosis effect of Semen Cuscutae in ovariectomized mice through inhibition of bone resorption by osteoclasts. *J. Ethnopharmacol.* **2022**, *285*, 13. https://doi.org/10.1016/j.jep.2021.114834.

19. Jiao, Y.; Wang, X.; Wang, Q.; et al. Mechanisms by which kidney-tonifying Chinese herbs inhibit osteoclastogenesis: Emphasis on immune cells. *Front. Pharmacol.* **2023**, *14*, 14. https://doi.org/10.3389/fphar.2023.1077796.

20. Tang, X.Y.; Huang, Y.X.; Fang, X.L.; et al. Cornus officinalis: A potential herb for treatment of osteoporosis. *Front. Med.* **2023**, *10*, 11. https://doi.org/10.3389/fmed.2023.1289144.

21. He, J.B.; Li, X.J.; Wang, Z.Y.; et al. Therapeutic Anabolic and Anticatabolic Benefits of Natural Chinese Medicines for the Treatment of Osteoporosis. *Front. Pharmacol.* **2019**, *10*, 23. https://doi.org/10.3389/fphar.2019.01344.

22. Yao, C.H.; Liu, B.S.; Liu, C.G.; et al. Osteogenic potential using a malleable, biodegradable composite added traditional Chinese medicine: In vitro and in vivo evaluations. *Am. J. Chin. Med.* **2006**, *34*, 873–886. https://doi.org/10.1142/s0192415x06004351.

23. Kang, W.Q.; Wei, P.F.; Ou, L.; et al. The mechanism study of inhibition effect of prepared Radix Rehmanniainon combined with Radix Astragali osteoporosis through PI3K-AKT signaling pathway. *Acta Cir. Bras.* **2022**, *37*, e371101. https://doi.org/10.1590/acb371101.

24. Hwang, J.H.; Kim, D.H.; Cho, Y.E.; et al. Yam-Derived Nanovesicles Stimulate Osteoblast Formation and Prevent Osteoporosis in Mice. *Ann. Nutr. Metab.* **2023**, *79*, 1090.

25. Hwang, Y. -H.; Kang, K. -Y.; Kim, J. -J.; et al. Effects of Hot Water Extracts from Polygonum multiflorum on Ovariectomy Induced Osteopenia in Mice. *Evid. Based Complement. Altern. Med. Ecam* **2016**, *2016,* 8970585.

26. Lee, W. C.; Guntur, A. R.; Long, F. X.; et al. Energy Metabolism of the Osteoblast: Implications for Osteoporosis. *Endocr. Rev.* **2017**, *38*, 255–266. https://doi.org/10.1210/er.2017-00064.

27. Xu, F.F.; Ding, Y.; Guo, Y.Y.; et al. Anti-osteoporosis effect of Epimedium via an estrogen-like mechanism based on a system-level approach. J. *Ethnopharmacol.* **2016**, *177*, 148–160. https://doi.org/10.1016/j.jep.2015.11.007.

28. Wei, C.; Wang, M.; Wang, X.-J. Evolutionary conservation analysis of human arachidonic acid metabolism pathway genes. *Life Med.* **2023**, *2*, lnad004. https://doi.org/10.1093/lifemedi/lnad004.